Spectral Imaging in a Snapshot

Andrew R Harvey[1]*, David W Fletcher-Holmes[1], Alistair Gorman[1],
Kirsten Altenbach[2], Jochen Arlt[2] and Nick D Read[2]

[1]School of Engineering and Physical Sciences, Heriot Watt University, Riccarton, Edinburgh, EH14 4AS UK
[2]COSMIC, The University of Edinburgh, James Clerk Maxwell Building, West Mains Rd., Edinburgh, EH9 3JG

*a.r.harvey@hw.ac.uk

ABSTRACT

We describe a new filter that simultaneously achieves spectral filtering and image replication to yield a two-dimensional, snapshot spectral imager. Filtering is achieved by spectral demultiplexing; that is without rejection of light; so optical throughput efficiency is, in principle, unity. The principle of operation can be considered as a generalisation of the Lyot filter to achieve multiple bandpasses. We report on the design and experimental implementation of an eight-band system for use in the visible. Proof-of-concept demonstrations are reported for imaging of the ocular fundus and microscopy of fluorescently labelled living cells.

1. INTRODUCTION

In this paper we describe a novel approach to spectral imaging based on image replication and polarising interferometry that offers the important and fundamental advantages of snapshot spectral imaging in two dimensions. Dubbed IRIS[1], the technique enables 2D spectral imaging with moderate spectral resolution and an instantaneous field of view in pixels that is reduced in proportion to the number of spectral bands. To highlight the advantages offered by IRIS we will first discuss the limitations of traditional approaches to spectral imaging.

During recent years many spectral imaging techniques have been described and it has become clear that all techniques involve some compromise with no single technique offering a panacea[2]. The optimum technique can be determined by a comparison of the requirements for an application and the capabilities of candidate techniques. Perhaps the simplest approach to spectral imaging is to spectrally filter either the source or scattered light; tuning or switching of the filter then enables a spectral data cube to be assembled in time sequence along the wavelength axis. For low-light applications, higher signal-to-noise ratios can be obtained using time-sequentially scanned Fourier-transform imaging spectrometers[3]. An alternative technique, favoured by the remote sensing community is to employ an imaging dispersive spectrometer to form a one-dimensional spectral image that is scanned linearly to construct the spectral data cube by scanning along the spatial dimension. A Fourier-transform equivalent of this technique has also been developed in which a one-dimensional array of spatial interferograms are recorded; an advantage of this technique is that the wide free-spectral range of Fourier-transform spectroscopy is obtained. A very important advantage of the one-dimensional spectral imager is that the full spectra are recorded in a snapshot, so the spectral distortion that can be introduced by imperfect coregistration of narrow-band images recorded in time-sequence is avoided[2].

A major disadvantage of these traditional techniques is that they are fundamentally unsuitable for recording phenomena that are changing on a timescale that is shorter than the duration required to reconstruct the data cube. Since this may be tens or hundreds of detector frames this is a major and fundamental restriction that imposes severe limitations in the application of spectral imaging to time-resolved imaging of biological and medical processes. Further problems arise when there is mutual translation between the scene to be spectrally imaged and the imager as occurs in spectral imaging of the eye[4,5,6,7] and spectral imaging surveillance from aerial platforms[8,9,10,11,12]. In both cases the major problem occurs because the translation is irregular and this can cause accurate coregistration of spectral images to be highly problematic. In the case where a one-dimensional image is scanned across the scene a penalty for imperfect coregistration is artefacts in the geometry of the spectral image, but for the case where the spectra are recorded in time sequence, imperfectly coregistered images introduce artefacts in the spectrum that reduce the effectiveness of spectral processing algorithms. In fact, to avoid this degradation typically requires coregistration of constituent images to be 1/20 of a pixel or better[2]. This can be somewhat challenging.

Where spectral imaging has been applied to applications requiring a snapshot capability it has been necessary to compromise resolution in either the spatial or spectral domain. Spectral imaging of fluorophors is important for time-resolved imaging of biological processes or for *in vivo* imaging of, for example, epithelia in cancer detection or in imaging of the retina. In the former case it is normal to reduce the spectral discrimination of the instrument to just two or three bands using multiple detectors and dichroic beam splitters that enable sufficient spectral discrimination. In the latter case, it is possible to use time-sequential recording of narrow-band images with subsequent coregistration employing natural or artificial land marks. For spectral imaging of the retina, veins tend to show high contrast across a wide spectral range and serve as excellent landmarks enabling accurate coregistration. In the absence of high-contrast natural landmarks, such as for imaging of the cervix, artificial landmarks may be added to the scene to enable subsequent coregistration[13]. There are significant difficulties and limitations introduced by *post facto* coregistration; even in well-controlled imaging configurations, there is often significant warping of the image due to relative movement between the imager and scene and biological samples are rarely totally stationary; for example, in coregistration of narrow-band retinal images recorded in time sequence it is apparent that in addition to relatively benign translational and rotational offsets between images, relative movement of the eye means that distortion of the eye-lens changes from image to image and movements of arteries in synchrony with the pulse means that coregistration artefacts will always be present.

A major advantage of using a one-dimensional spectral imager, as has been demonstrated in aerial hyperspectral surveillance and spectral imaging of the eye, is that this technique does not suffer from temporally induced spectral misregistration. One-dimensional hyperspectral imagers have been implemented in retinal imaging where they are co-aligned, using beam-splitter optics, with a conventional monochrome or colour CCD camera[14,15] , but in this case the imagers record a hyperspectral image of a line across a specific structure; this can enable, for example, oximetry in blood vessels, but is less well suited to screening purposes.

Spectral imaging techniques that record a two-dimensional spectral image in a snapshot are notable by their absence. The traditional trichromatic colour camera is a prominent exception, but the basic principle used - multiple dichroic beamsplitters to demultiplex or filter the light - is fundamentally unsuitable to imaging in more than a few spectral bands. An elegant technique known as Computer Tomographic Imaging Spectroscopy (CTIS) employs a diffractive optical element in the pupil plane of a conventional imager to spectrally disperse the image at the detector; computer inversion algorithms reconstruct the spectral data cube from a single snapshot image[16]. We report here a two-dimensional snapshot technique, called IRIS (Image Replicating Imaging Spectrometer) that also records a spectral data cube directly onto a single, conventional detector array. There is however no overlap of images and, in principle, there is no dispersion of the image, so there is no need to further process the data to produce a spectral image. Because there is no inversion of the data, IRIS does not suffer the compromised noise performance that is introduced by inversion of data in the shot-noise-limited regime[2]. Furthermore, all of the detector pixels are used so that the number of voxels in the data cube is equal to the number of detectors in the detector array.

The snapshot capability offers the following key advantages:

- Time-resolved spectral imaging of transient phenomena is possible
- No temporally induced spectral misregistration or geometric distortion is introduced
- There are no multiplex losses so signal throughput can be very high
- There are no moving parts so reliability and robustness is high

The ability to record 2D snapshot spectral images is a fundamental advantage in terms of its ability to record transient or time-varying scenes, however the multiplex advantage depends upon the application. Fundamentally, the number of pixels in the spectral image cube (that is voxels) that can be recorded in a snapshot is limited by the space-bandwidth product (that is, the number of detector pixels) of the detector array, or arrays, that are used. The application of IRIS involves the snapshot imaging of N narrow-band non-overlapping images onto a single detector array so that there is a trade off between spectral resolution and field of view. Although, in terms of the number of pixels per image, the field of view of IRIS is reduced in comparison to a spectral imager using spectral-temporal multiplexing, for those applications for which it is sufficiently extended without the need for spatial scanning, there is a very significant multiplex advantage; as high as N in comparison to a spectrally multiplexed technique. If, however, a need for an extended field of regard requires scanning of the IRIS imager than this is in effect spatial multiplexing and the full multiplex advantage will not be obtained.

2. IMAGE REPLICATION IMAGING SPECTROMETER: PRINCIPLE OF OPERATION

The image replicating imaging spectrometer can be considered as a generalisation of a Lyot filter; this enables high efficiency spectral demultiplexing of broadband light. The Lyot filter[17,18,19,20], as used for many years in astronomy,

employs polarising interferometry within multiple waveplates to yield a narrow-band filter suitable for recording monochromatic images. Light not transmitted by the Lyot filter is absorbed by film polarisers. To generalise the Lyot filter, Wollaston prism polarising beam splitters are used in place of film polarizers enabling spectral images to be recorded simultaneously in several pass-bands without rejection of light. Prior to describing the principle of operation of IRIS we will first consider the principle of a conventional Lyot filter.

A Lyot filter, as illustrated in Figure 1, is composed of multiple waveplates sandwiched between co-aligned linear polarisers aligned to pass light polarised at 45º to the fast axis of each waveplate. The linearly polarised light propagating through the waveplate is resolved into orthogonally polarised components that interfere at the output analysing polariser with a mutual optical path difference $\Delta=(n_o-n_e)t$ between the orthogonal components where n_o and n_e are the ordinary and extraordinary refractive indices of the waveplate and t is its thickness. The output polariser is aligned with the input polariser so that the overall transmission function of the polariser-waveplate-polariser assembly is proportional to $\cos^2(\pi\nu\Delta)$ where $\nu=1/\lambda$ is optical frequency. A Lyot filter consists of an assembly of multiple polariser/waveplate combinations where the ratio between the thicknesses of consecutive waveplates is a factor of two. The spectral transmission function of an n-waveplate Lyot filter is thus the product of the transmission functions of all constituent waveplate/polariser assembly and is given by

$$T(\nu)=\prod_{i=1}^{n}\cos^2(i\pi\nu\Delta)\cdot \quad \textbf{(1)}$$

A four-waveplate Lyot filter is depicted in Figure 1. A generalisation of this technique is employed with the IRIS concept described here whereby the film polarisers are replaced with Wollaston prism polarising beam splitters as shown in Figure 2 (a). The use of a polarising beam splitter means that after transmission through each waveplate the light is resolved into polarisations both, aligned with, and orthogonal to, the input polarisation state. As with the Lyot filter, for the co-polarised component the transmission function is given by $\cos^2(\pi\nu\Delta)$; for the cross-polarised component the transmission function is $\sin^2(\pi\nu\Delta)$. Furthermore, these two orthogonally polarised components are displaced in angle by the beam-splitting action of the Wollaston prism and this enables two spatially separated and spectrally filtered replica images to be formed. Subsequent Wollaston prism polariser pairs further spectrally filter and replicate the images. After transmission through n Wollaston prism polariser pairs 2^n replicated images are formed, each with a unique product of $\sin^2(i\pi\nu\Delta)$ and $\cos^2(i\pi\nu\Delta)$ transmission functions. It can be seen then that the IRIS technique simultaneously replicates the image formed at the field stop whilst applying a unique spectral filtering function to each image; this filtering function is determined by how light arriving at each image was steered and spectrally modulated. IRIS thus performs the function of an imaging spectral demultiplexor with image components lying within a spectral band tending to be steered to a particular part of the detector array. The images at the detector array are prevented from overlapping by a field stop.

The orientation and magnitude of the splitting angles of the Wollaston prisms determines the locations of the replicated images at the detector; each image can be identified by a vector $\{p(1), p(2).. p(n)\}$ where each element of the vector identifies whether the image is due to refraction in a positive or negative direction at each Wollaston prism. In general, the transmission function for each image at location $\{p(1), p(2).. p(n)\}$ in the image plane can be written as

$$T_{p(1),p(2)..p(n)}(\nu)=\prod_{i=1}^{n}\Omega_{a(n)}(i\pi\nu\Delta) \quad \textbf{(2)}$$

where $a(i)$ refers to either co-polar or cross-polar transmission between Wollaston prisms, so that the respective transmission functions for co-polar and cross-polar transmissions through waveplate i sandwiched between polarisers i-1 and i are

$$\Omega_{a(i)=co-polar}(x)=\cos^2(x),$$

$$\Omega_{a(i)=cross-polar}(x)=\sin^2(x) \quad \textbf{(3)}$$

where suffix i=0 indicates the input polarizer and all other values indicate Wollaston prism polarizers. The spectrum associated with each individual image replication is determined by the vector $\{a(1), a(2),.. a(n)\}$ appropriate for each image replication. Since spectral filtering and image replication operations commute, the order of the vector elements is

not important; it will always result in the same combination of 2^n products of the n pairs of $\cos^2$ and $\sin^2$ functions being applied at the image. For an IRIS employing three Wollaston prisms the eight pass-bands pass-band are given by

$$
\begin{aligned}
T_1(\nu) &= \cos^2[\pi\nu\Delta]\cos^2[2\pi\nu\Delta]\cos^2[4\pi\nu\Delta] \\
T_2(\nu) &= \cos^2[\pi\nu\Delta]\cos^2[2\pi\nu\Delta]\sin^2[4\pi\nu\Delta] \\
T_3(\nu) &= \cos^2[\pi\nu\Delta]\sin^2[2\pi\nu\Delta]\cos^2[4\pi\nu\Delta] \\
T_4(\nu) &= \cos^2[\pi\nu\Delta]\sin^2[2\pi\nu\Delta]\sin^2[4\pi\nu\Delta] \\
T_5(\nu) &= \sin^2[\pi\nu\Delta]\cos^2[2\pi\nu\Delta]\cos^2[4\pi\nu\Delta] \\
T_6(\nu) &= \sin^2[\pi\nu\Delta]\cos^2[2\pi\nu\Delta]\sin^2[4\pi\nu\Delta] \\
T_7(\nu) &= \sin^2[\pi\nu\Delta]\sin^2[2\pi\nu\Delta]\cos^2[4\pi\nu\Delta] \\
T_8(\nu) &= \sin^2[\pi\nu\Delta]\sin^2[2\pi\nu\Delta]\sin^2[4\pi\nu\Delta]
\end{aligned}
\qquad \textbf{(4)}
$$

As can be seen the first term is identical to the spectral transmission function of the equivalent Lyot filter. Due to the wide spectral range of IRIS it is necessary to use the dispersive variation of Δ with wavenumber when evaluating (4). In Figure 3(a) are shown the eight calculated transmission functions for an eight-band IRIS employing quartz waveplates with thicknesses for the three waveplates of t=120, 240 and 480 μm. The resultant pass-bands are bell-shaped and exhibit significant sidelobes. For visible band imaging, quartz is an ideal material for the waveplates since its relatively small birefringence yields relatively thick and robust waveplates with relaxed manufacturing tolerances.

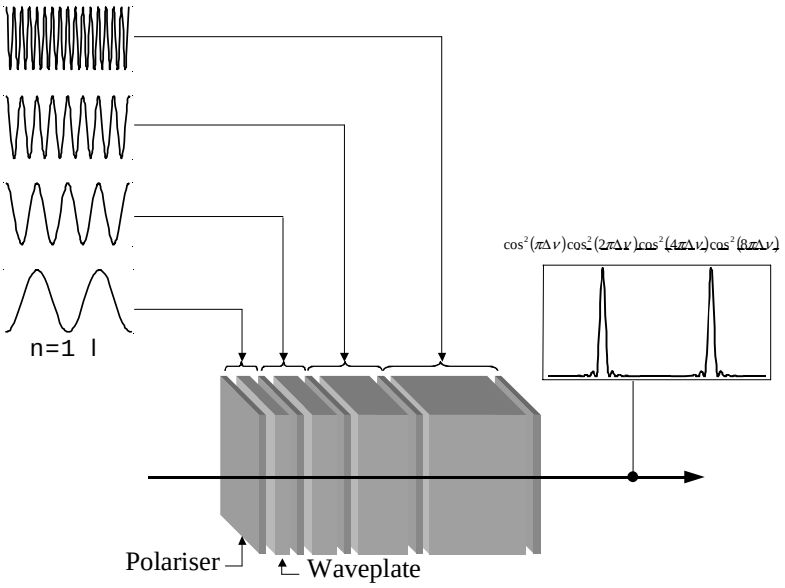

Figure 1 Depiction of the principle of operation of the Lyot filter

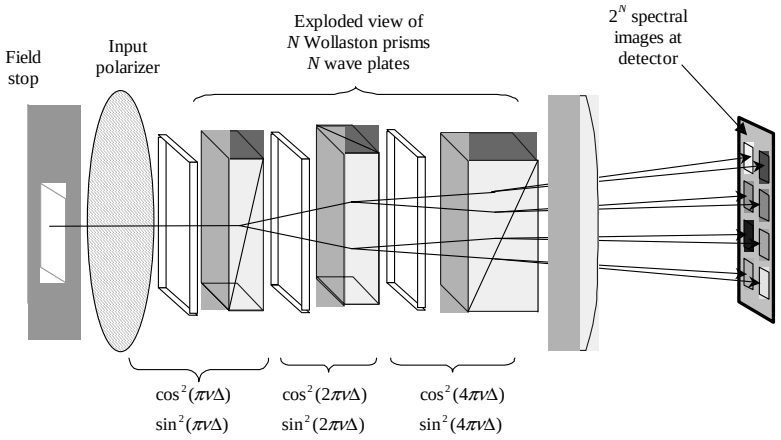

Figure 2 Depiction of principle of operation of Image replication imaging spectrometer

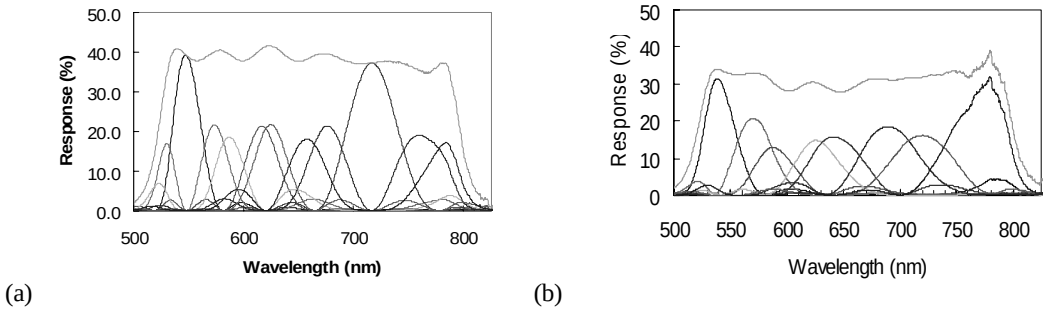

Figure 3 Transmission functions for each of eight images using (a) theoretical transmission for waveplates with thicknesses related by a simple factor of 2 and (b) measured transmission for waveplates optimised in thickness to produce transmission curves with maximum fractional power in the main lobes.

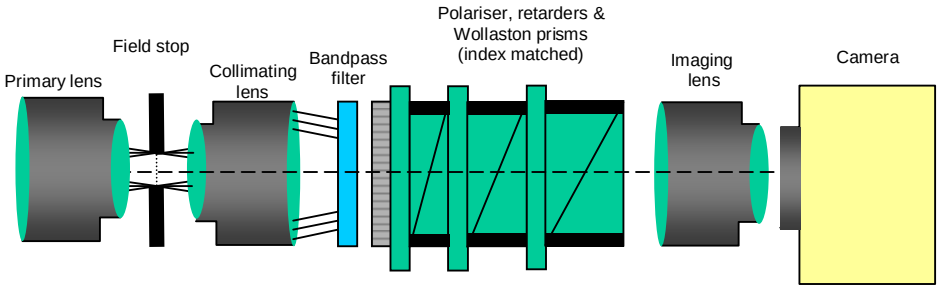

Figure 4 (a) Schematic of the implementation of the 8-channel IRIS concept within a spectral imager

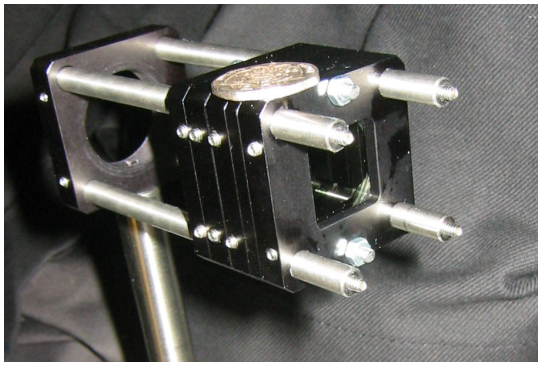

Figure 5 Assembled Wollaston prisms and waveplates for an 8-channel IRIS

Modification of the thicknesses of the waveplates can improve the characteristics of the passbands; optimisation of the thickness values against a merit function related to the desired spectral filtering characteristics can suppress the sidelobes. We have found that a merit function that maximises the average optical power in the main peaks of each transmission function (and hence minimising the average sidelobe power) yields spectral curves that are efficient at maximising the separation of the spectra of typical materials in spectral hyperspace. It is more appropriate then to replace equation (3) by

$$\Omega_{a(i)}(\nu) = \cos^2(\pi \nu b(\nu) t_i)$$

$$\Omega_{a(i)}(\nu) = \sin^2(\pi \nu b(\nu) t_i) \qquad \textbf{(5)}$$

where t_i is the thickness of waveplate i and $b(\nu)$ is the birefringence at wavenumber ν.

Optimisation of the above system using this technique yielded thicknesses for the quartz waveplates of t=121, 176 and 350 μm. Measured transmission functions under polarised illumination for an optimised eight band imager, based on these thicknesses are shown in Figure 3(b). The spectral transmission is restricted by low-pass and high-pass edge filters. The overall transmission efficiency of this system is limited to about 45% in polarised light; the dominant contributions arise from the dichroic input polariser and losses in the two edge filters. The use of a high-efficiency single element bandpass filter will increase transmission to greater than 80%.

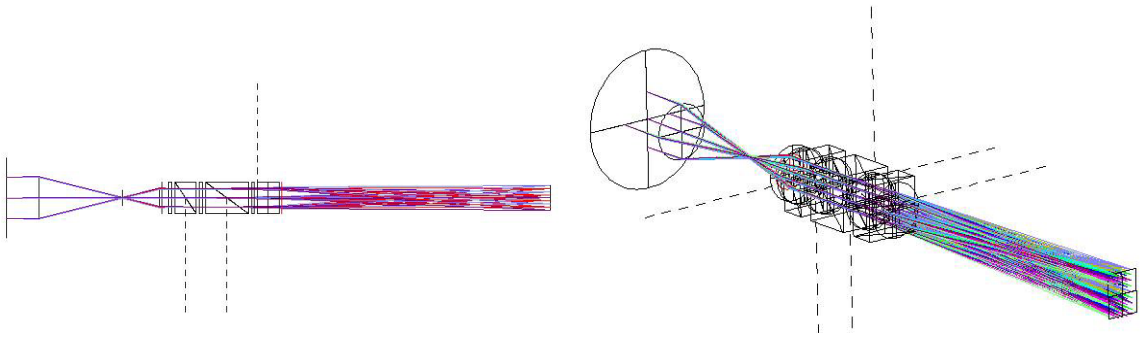

Figure 6 Ray trace of 8-channel IRIS system.

Whilst it is not possible to synthesis the contiguous rectangular functions typically employed in spectrometry, in many cases this will not significantly reduce spectral discrimination performance of IRIS. A heuristic illustration of this is the good spectral discrimination possible with the human visual system which also employs broad overlapping and bell-shaped response curves. A more quantitative appraisal is the evaluation of the separation of recorded spectra in spectral space. For typical smoothly varying spectra, the separation of spectra in spectral space is reduced by about 10% with respect to the separation obtained by an ideal spectrometer whilst the spectral throughput is, for an eight-channel system, eight-fold higher, resulting in a net improvement in signal-to-noise ratio by a factor of more than seven in comparison to a spectrally multiplexed system

3. EXAMPLE RESULTS FOR EIGHT-BAND IRIS SYSTEMS: SPECTRAL RETINAL IMAGING AND SPECTRAL MICROSCOPY

A schematic of an assembled, 8-channel IRIS system is shown in Figure 4. This consists of an image relay system with an intermediate image plane. The IRIS components depicted in figure 3 are located close to the pupil plane of the image relay system, thus they replicate the image formed at the field stop onto the detector array. The field stop, or intermediate focal plane, is required to prevent overlapping of the replicated images at the detector plane. The IRIS birefringent elements are assembled into a common block with index matching fluid to reduce stray reflections and to reduce the effect of non-flatness of the birefringent elements. A photograph of the assembled IRIS block is shown in Figure 5 with together a UK 20p coin for scale.

A snapshot spectral imaging capability can be readily added to a conventional imaging system; we report here proof-of-concept experiments in which eight-band IRIS systems have been fitted to (a) a conventional retinal camera[21] and (b) a conventional multi-port microscope[22].The IRIS systems, as shown in Figure 4, are assembled using a modular optical bench system. In each case these were mounted using a conventional C-mount on the imaging systems (either the retinal imager or microscope) so that the input 'intermediate focal plane' of IRIS coincided with the output image plane of the imaging system. The image at this output plane was then spectrally demultiplexed by IRIS into eight narrow-band images recorded on a cooled CCD camera. The spectral filtering function of the IRIS system varied between the two demonstrations.

In the case of the retinal camera the spectral filtering was designed to enable oximetry within retinal blood vessels; the dominant factor determining the reflectivity of blood vessels is the absorption spectrum of haemoglobin. As can be appreciated from the data presented in Figure 7(a), for wavelengths less than about 580 nm, the optical depth for both oxygenated and deoxygenated blood is significantly less than the diameter of all but the smallest blood vessels and so both oxygenated and deoxygenated blood within blood vessels are effectively opaque. Between 580 nm and 620 nm there is a rapid decrease in the absorption by oxygenated blood so that at 620 nm the optical depth considerably exceeds the thickness of all blood vessels and the blood column becomes effectively transparent whilst for deoxygenated blood the blood column remains effectively opaque. Monitoring the optical density of blood at a range of wavelengths between 580 and 620 nm enables the effect of blood oxygenation to be separated out from variability introduced by other pigments, such as melanin, to enable blood oxygenation to be calculated. An IRIS system was designed with quartz waveplates with thicknesses optimised to produce eight, approximately equally spaced, spectral pass-bands within the range 580-620 nm. The bandpass filter was placed in the illumination path to reduce the light intensity at the eye and to reduce the effect on image quality. The measured spectral passbands are shown in Figure 7(b). A single frame showing the eight replicated narrow-band images is shown in Figure 8(a). The systematic reduction of optical density with increasing wavelength for some of the blood vessels can be clearly seen and identifies these as arteries carrying oxygenated blood. Although flash-lamp illumination was used to record these images, it was also possible to record real-time spectral images of the retina, albeit of lower quality, using only low-power, tungsten filament inspection lamp.

In a similar fashion, as an initial part of a programme of work to monitor multiple fluorophors using real-time spectral imaging, investigative multi-spectral imaging experiments were conducted using an IRIS system mounted on a conventional epi-fluorescence microscope. The passbands of the IRIS system were those shown in Figure 3b. Since fluorescence was to be imaged, the bandpass filter was in this case located in the pupil plane of the image relay optics. The recorded images are shown in Figure 9. In Figure 9(a) eight narrow-band images can be seen of a branched filamentous cell of the fungal plant pathogen *Cochliobolus heterostrophus* stained with the pH-sensitive dye carboxy-SNARF-1. The fluorescence spectrum of carboxy-SNARF-1 changes in response to changes in pH. Using IRIS, changes in the fluorescence spectrum of this dye can be monitored in real time and, after appropriate calibration, be used to precisely quantify intracellular pH[25]. Figure 9b shows eight narrow-band images of germinating spores of the fungus *Neurospora crassa* labelled with the green fluorescent protein and the membrane-selective dye, FM4-64, after blue UV excitation. The green fluorescent protein is only detected at 540 nm whilst FM4-64 is best detected between 580 and 680

nm. Simultaneous spectral imaging will be extremely useful for imaging cells labelled with multiple probes, especially where the fluorescence spectral bandwidths are narrow (e.g. as in the case of quantum dots[26]).

4. CONCLUSIONS

We have described a new concept in spectral imaging instrumentation that combines polarising interferometry and polarising beam splitters to simultaneously implement image replication and spectral demultiplexing. This enables snapshot spectral imaging in two dimensions, promising the extension of spectral imaging to transient and unstable phenomena. Moreover, in contrast to other high throughput techniques there is no data inversion and so the associated SNR advantage is retained even in shot-noise limited imaging conditions.

Preliminary *in vivo* images of the retina have been recorded that will enable quantitative blood oximetry, and some live-cell imaging has been recorded. The snapshot capability is vital in both these cases in that it removes significant and fundamental problems associated with coregistration of images and calibration.

Future work will involve development of spectral unmixing algorithms and optimisation of the IRIS technique, in terms of both the shape and number of spectral bands for specific applications.

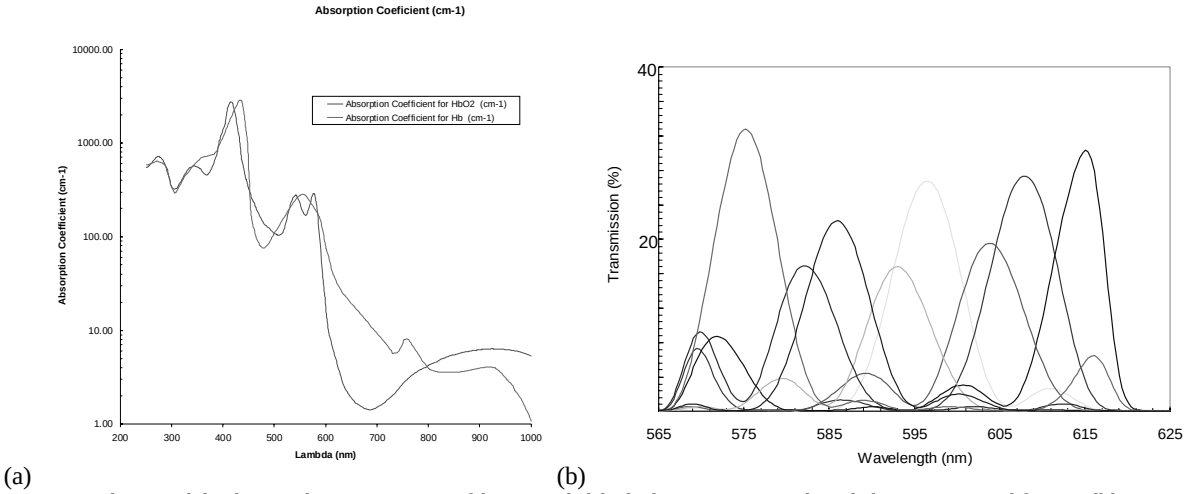

(a) (b)

Figure 7(a) Absorption spectrum of haemoglobin in its oxygenated and deoxygenated forms (b) spectral transmission functions of IRIS system designed for retinal blood oxymetry

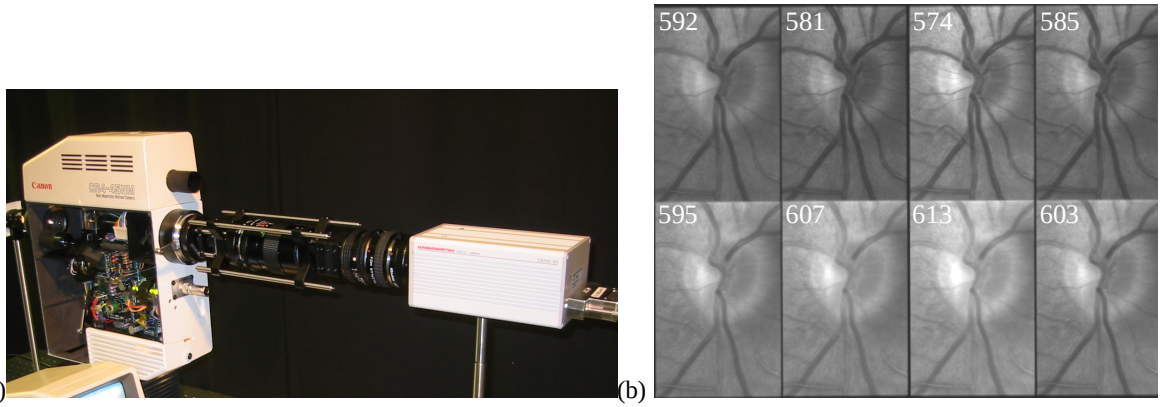

(a) (b)

Figure 8 Eight narrow-band images of an optic disc recorded at the detector

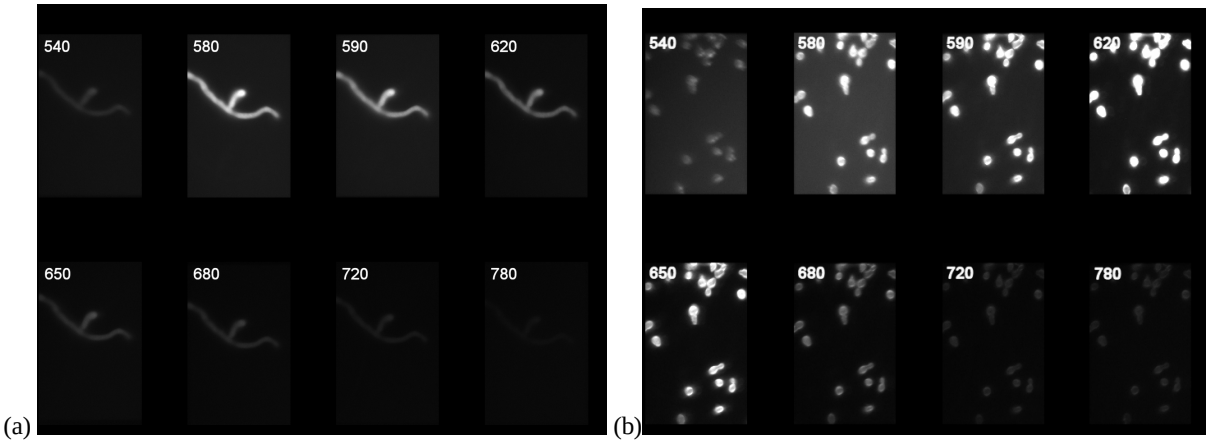

Figure 9 Eight narrow-band images of (a) *Cochliobolus heterostrophus* labelled with carboxy-SNARF-1 and (b) *Neurospora crassa* labelled with the green fluorescent protein and FM4-64

5. ACKNOWLEDGEMENTS

This work was carried out with funding from the Engineering and Physical Research Council, The Royal Society. and BAE systems.

6. REFERENCES

[1]A R Harvey, D.W. Fletcher-Holmes, *Imaging Apparatus*, Patent WO2004 005870 A1, (2004)
[2] A.R. Harvey, J. Beale, A.H. Greenaway, T.J. Hanlon and J. Williams, "Technology options for imaging spectrometry" *Proc SPIE*, 4132, pp13-24, 2000
[3] A R Harvey, D W Fletcher-Holmes, *Birefringent Fourier-transform imaging spectrometer*, Optics Express **12**, 22, pp 5368-74, (2004)
[4] A.R.Harvey, J.Lawlor, A.I.McNaught, J.W.Williams and D.W.Fletcher-Holmes. *Hyperspectral imaging for the detection of retinal diseases.* SPIE 4816-37, pp325-335, Proc. Conference on Imaging Spectrometry VIII, Seattle July 7-11, 2002.
[5] V.Papadakis, M.P. Karavellas, M.K. Tsillimbaris, C.Balas, and I.G.Pallikaris, *A hyperspectral imaging fundus camera for the detection and characterisation of retinal lesions*. The Association for Research in Vision and Ophthalmology. Ocular Imaging, 4362-B331, pp. 174, May 5-10, 2002.
[6] J.Lawlor, D.W.Fletcher-Holmes A.I.McNaught A.R.Harvey. *In vivo hyperspectral imaging of human retina and optic disc.* The Association for Research in Vision and Development, Anatomy and Physiology/Retinal Cell Biology. 4350-B319. Annual Meeting Fort Lauderdale, Florida May 5-10, 2002
[7] F.C. Delori, *Spectrophotometer for noninvasive measurement of intrinsic fluorescence and reflectance in the ocular fundus*, Applied Optics, Vol. 33, pp.7439-7452, 1994.
[8] P. Mouroulis, *Spectral and spatial uniformity in push-broom imaging spectrometers*, Imaging spectrometry V, SPIE 3753 pp 133-141 (1999)
[9] G.R.O Vane, T G Green, H T Chrien, E G Hanson, W M Porter,*The airborne visible/infrared imaging spectrometer (AVRIS)* Remote Sen. Environ., **44**, pp127-143, (1993)
[10] T Wilson, C Davis, *Naval EarthMap Observer (NEMO) Satellite*, Imaging Spectrometry V, SPIE 3753, pp 2-11 (1999)
[11] J A Hackwell et al, *LWIR/MWIR imaging hyperspectral sensor for airborne and ground-based remote sensing*, Proc. SPIE 2819, pp 274-283 (1995)
[12] R W Basedow, D C Carmer, M L Anderson, *HYDICE system implementation and performance*, SPIE 2480, pp 258-267 (1995)
[13] A. Agrawa, T. Harrell, S. Bambo,, M. Faupel, D. Ferris Multimodal multispectral imaging of the cervix in vivo for the detection of neoplasia,pp68 Biomarkers and Biological Spectral Imaging, G.H. Bearman, D.J. Bornhop, R.M. Levenson, Editors, Proceedings of SPIE Vol. 4259 (2001)
[14] M Hammer, D Schweitzer, L Leistritz, M Scibor,K Donnerhacke,‡ and J Strobel, *Imaging spectroscopy of the human ocular fundus in vivo*, journal of biomedical optics 2(4), 418–425 (1997)
[15] G. Zamora, P. W. Truitt, S. C. Nemeth, Balaji Raman, Peter Soliz, *Hyperspectral image analysis for ophthalmic applications*, Ophthalmic Technologies XIV, edited by Fabrice Manns, Per G. Söderberg, Arthur Ho, Proceedings of SPIE Vol. 5314 (SPIE, Bellingham, WA, 2004)

[16] M R Descour, C E Volin, E L Dereniak, K J Thome, A B Schumaker, D W Wilson, P D Maker, *Demonstration of a high speed non-scanning imaging spectrometer*, Optics letters, **22**, 16, pp 1271-1273 (1997)
[17] B. Lyot, *Filter monochromatique polarisant et ses applications en physique solaire*, Ann. Astrophys. 7, 32 (1944)
[18] B. Lyot, *Optical apparatus with wide field using interference of polarized light*, C.R. Acad. Sci. (Paris) 197, 1593 (1933).
[19] Y. Ohman, *A new monochromator*, Nature 41, 157, 291 (1938).
[20] Y. Ohman, *On some new birefringent filter for solar research*, Ark. Astron. 2, 165 (1958).
[21] Canon CF20
[22] Nikon TE2000U inverted epi-fluorescence microscope
[25] R.M. Parton, S. Fischer, R. Malhó, O. Papasouliotis, T.C. Jelitto, T. Leonard, N.D. Read *Pronounced cytoplasmic gradients are not required for tip growth in plant and fungal cells*, J. Cell Sci. 110, 1187 (1997)
[26] T.M. Jovin *Quantum dots finally come of age*, Nat Biotechnol. 21, 32-33 (2003)